forests

MDPI

Article

Studies of the Photoprotection of Radiata Pine Wood Using Photocatalytic Nanoparticles

Vicente A. Hernandez [1,2,*], Romina Romero [3,*], Nicole Sagredo [2], David Contreras [3] and Philip D. Evans [4]

[1] Departamento de Manejo de Bosques y Medio Ambiente, Facultad de Ciencias Forestales, Universidad de Concepción, Victoria 631, Concepción 4070386, Chile
[2] Centro de Biotecnología, University of Concepción, Barrio Universitario S/N, Concepción 4070386, Chile
[3] Departamento de Química Analítica e Inorgánica, Facultad de Ciencias Químicas, Universidad de Concepción, Edmundo Larenas 129, Concepción 4070371, Chile
[4] Department of Wood Science, Faculty of Forestry, University of British Columbia, 2424 Main Mall, Vancouver, BC V6T 1Z4, Canada
* Correspondence: vhernandezc@udec.cl (V.A.H.); rominaromero@udec.cl (R.R.); Tel.: +56-41-2661449 (V.A.H.)

Abstract: In this work, TiO_2 and ZnO nanoparticles of different sizes and crystallographic configuration were used to protect wood surfaces against UV radiation. The sizes and levels of photoactivity of the nanoparticles were measured in vitro by transmittance electron microscopy and electron paramagnetic resonance spectroscopy, and then they were impregnated into radiata pine samples. The production of aromatic radicals, absorbance of UV and visible light, and chemical and color changes of treated and untreated wood surfaces were assessed after UV irradiation. Results show that nanoparticles that were less photoactive were better at reducing the production of organic radicals and the chemical and color changes on wood surfaces subjected to UV. Similarly, smaller nanoparticles (40 nm) were better at reducing photochemical reactions than larger (100 nm) nanoparticles. In terms of the crystallographic configuration of nanoparticles, differences in the production of phenoxy radicals were verified only for short-term exposure. Previous research revealed that certain levels of photoactivity in TiO_2 nanoparticles may contribute to decreases in the photodegradation of wood surfaces possibly by an electron sink mechanism. Our observations indicate that this is unlikely to occur in the presence of highly photoactive nanoparticles.

Keywords: wood photoprotection; titanium dioxide; zinc oxide; photocatalysis; nanoparticles

Citation: Hernandez, V.A.; Romero, R.; Sagredo, N.; Contreras, D.; Evans, P.D. Studies of the Photoprotection of Radiata Pine Wood Using Photocatalytic Nanoparticles. *Forests* **2022**, *13*, 1922. https://doi.org/10.3390/f13111922

Academic Editors: Jorge Santos and Danilo Escobar-Avello

Received: 12 October 2022
Accepted: 12 November 2022
Published: 16 November 2022

1. Introduction

The exposure of wooden elements to the action of environmental factors significantly modifies their surface structure, this effect is known as weathering [1]. Solar radiation has been identified as the most damaging factor during weathering of wood. Solar radiation is absorbed by all wood's constituent polymers, but particularly by lignin, which is severely affected [2–4]. The critical wavelengths to break the most important chemical bonds in wood polymers are 346, 334, and 289 nm. These wavelengths are found in the UV component of solar radiation and affect the carbon–carbon, carbon–oxygen and carbon–hydrogen bonds, respectively [3,5].

Exposure to UV radiation and other environmental factors adversely affects the surface properties of wood and the performance of coatings [1–3,6]. Hence, there has been significant interest in the development of treatments to photostabilize wood and also on the evaluation of the photoprotective effects of wood modification or treatment of wood with biocidal preservatives [3,6–8]. Surface treatments that are the most effective at improving the performance of coatings are transition metal compounds that photostabilize lignin [6,9–11], organic UV absorbers and hindered amine light stabilizers [6,12,13], and reflectors and pigments [14,15]. More recently, there has been significant interest in inorganic nanoparticles (NPs) as photoprotective treatments for wood surfaces [16].

NPs can effectively reduce color changes due to photodegradation when applied directly or in combination with coating systems to wood surfaces [17]. It is commonly accepted that NPs protect wood against UV radiation because of their ability to block, scatter, and absorb UV [18]. However, their modes of action have not been fully explored. For example, at nanoscale, the absorption of UV radiation by inorganic NPs involves the production of radical species in the presence of oxygen and water [19–23]. This effect is known as photocatalysis, and there is no general agreement on whether such species resulting from the presence of NPs can induce or accelerate chemical changes on wood surfaces during UV exposure [24–26].

The level of photoactivity of inorganic nanoparticles can be tailored by including different elements in their composition and by the synthesis of particular nanostructures of different sizes. For example, highly efficient photocatalytic NPs have been experimentally produced and used for the degradation of dyes and pollutants, achieving activation even under visible light with different principles of action [27–29]. The high efficiency of these photosensitizers produces large concentrations of radical species that are highly effective at degrading organic materials such as lignin on wood surfaces.

In our previous work, we suppressed the photocatalytic activity of TiO_2 NPs prior to testing their effects on wood surfaces exposed to artificial UV radiation (340 nm). We assessed whether the suppression of free radical production due to photocatalysis had a significant effect on the final color and chemical stability of wood surfaces. Surprisingly, we found that the suppression of photocatalytic activity increased the level of aromatic radicals, measured by electron paramagnetic resonance (EPR), and color changes during long-term UV exposure. We theorized that, without modifications that could suppress its photoactive nature, the ability of TiO_2 to act as an electron sink in its rutile phase might explain these results. More specifically, the holes and excited electrons that migrate to the surface of the nanoparticles when irradiated with UV may interact with the aromatic radicals caused by the UV degradation of lignin, interrupting further oxidative reaction with other wood's components, hence slowing color changes. Additional research is necessary to test this hypothesis [30].

In this work, we extend our previous research by testing inorganic NPs of different types (TiO_2 and ZnO), sizes (40 to 280 nm), and crystallographic configuration (anatase and rutile). The NPs were characterized for their size and level of photoactivity in vitro by transmittance electron microscopy (TEM) and electron paramagnetic resonance (EPR), and then they were impregnated into wood samples. During the experiments, the production of aromatic radicals, and chemical and color changes of the treated and control surfaces, was assessed upon UV exposure (340 nm). In addition, surfaces were tested for their ability to absorb UV and visible light after UV irradiation.

As a biomaterial made of different organic polymers, wood represents a complex substrate. Therefore, the generation of new insights into its photochemical behavior, particularly in the presence of NPs with different levels of photocatalytic activity, is vital for the development of new and more effective photoprotective treatments.

2. Materials and Methods

2.1. Nanoparticles

ZnO and TiO_2 NPs (>99% purity) were acquired from US Research Nanomaterials, Inc. The NPs were white, semi-spherical, and varied in size from 40 to 280 nm. We used ZnO 35–45 nm (ZnO35), ZnO 80–200 nm (ZnO80), TiO_2 anatase 40 and 100 nm (A40 and A100, respectively), and TiO_2 rutile 50 and 100 nm (R50 and R100, respectively). Anatase and rutile are the two most widely used mineral forms of titanium dioxide in material science and industry [31].

2.2. Photoactivity Tests on Nanoparticles

A Bruker EMX micro with ER 4119HS cavity electron paramagnetic resonance (EPR) equipment was used to test the photocatalytic activity of ZnO and TiO_2 NP. The kinetics

of adducted OH radical intensity were assessed during 60 min of direct irradiation with artificial UV light at 340 nm [17]. In the experiments, 2.5 mL (0.01 mol·L^{-1}) of 5,5-dimethyl-1-pyrroline N-oxide (DMPO, Sigma-Aldrich) was added to 1.23 × 10^{-4} mol of active NP. The dispersions were then sonicated and exposed to UV light under stirring; aliquots were taken after 5, 7.5, and 10 min of exposure. Thereafter, sampling was carried out every ten minutes until completion of 60 min of exposure. Concentration of ·OH radical intensity was measured by adjusting the magnetic field to the dominant peaks of the adduct spectrum. The change in the absorption in such a field was measured as the ·OH concentration, since the height of this peak is proportional to the amount of DMPO/OH [32].

A different EPR experiment was carried out to look for free radicals in wood surfaces treated with NPs and exposed to UV radiation. Radiata pine (*Pinus radiata* D. Don) samples (1 × 1 × 10 mm^3) were prepared from a sapwood board previously conditioned to 12% moisture content. Different samples (n = 3) were immersed, under stirring, for 5 h in ethanol dispersions (1%) of the different NPs and then dried at room temperature (24 h). These NP-impregnated wood samples were then exposed to artificial UV radiation of 340 nm. After 120, 1440, and 2800 min of exposure, samples were collected and inserted in the EPR equipment to measure the intensity of free radicals produced.

All EPR measurements were performed at 2000 mW microwave power, 100 kHz modulation frequency, 3515 G center field with a sweep width of 200 G, and receiver gain of 20 dB with 30 s sweep time.

2.3. Treatment of Wood Samples with Nanoparticles

Wood samples (n = 3) were cut and planed to 10 × 40 × 80 mm^3 (tangentially oriented) from conditioned defect-free radiata pine boards. Ethanolic dispersions of different NPs were prepared at a concentration of 1% and then vacuum impregnated into wood samples (−0.1 MPa, 30 min). Vacuum impregnation allowed a shorter treatment time, while ensuring the penetration of nanoparticles into sub-surface wood cells (checked by scanning electron microscopy, Figure S1). The experiment involved the application of one type of nanoparticle to individual samples and also included control samples without treatment. Control and treated samples were dried at room temperature for 24 h, and then conditioned (21 °C, 65% relative humidity) for two weeks in a dark room before their exposure to UV radiation. Weight gain due to the impregnation process was determined in additional samples by contrasting the anhydrous weight of samples before and after impregnation.

2.4. UV Exposure

Control and treated wood samples were exposed to 340 nm-UV radiation in a custom-built exposure unit located in the "Wood Protection Laboratory", Facultad de Ciencias Forestales, Universidad de Concepción, Chile, according to Hernandez et al. (2015 and 2020) [30,33]. The exposure unit contained 4 UV tubes (48 inches in length), 40 W (Q-Lab Corp., Cleveland, OH, USA). Temperature and irradiation doses were 40 °C and 2.65 W/m^2, respectively, while the distance between the surfaces and tubes was maintained at 50 mm. Samples were randomly sorted for exposure and re-arranged every 24 h until the end of the exposure period. After 120, 1440, and 2880 min of exposure, samples were collected, and the color and chemical changes at their exposed surfaces were measured.

2.5. Wood Surface Color Change Measurements

The color of wood samples exposed to artificial UV radiation was measured after 120, 1440, and 2880 min of exposure using a spectrophotometer (Konica-Minolta CM-5). Color is expressed using CIE L*a*b* coordinates. Differences in the color components corresponding to lightness (ΔL*), greenness–redness (Δa*) and blueness–yellowness (Δb*) were calculated by subtracting the color value before exposure from the color value after exposure. A unit of change in any component represents a perceptible difference for objects having uniform coloration under ideal lighting [34]. In addition, digital images of the samples before and after the exposure were taken with a desktop scanner Epson Perfection V370 Photo.

2.6. Chemical Changes on Wood Surfaces

Chemical changes, before and after 2880 min of exposure on untreated and NP-treated surfaces, were evaluated by Fourier transform infrared spectroscopy–attenuated total reflectance (FTIR–ATR). FTIR–ATR spectra were acquired by using a single-bounce attenuated total reflectance accessory (Bruker Optic Pvt. Ltd., Billerica, MA, USA). Acquired spectra represented 36 accumulations, at 4 cm^{-1} resolution, in the fingerprint region from 1500 to 500 (cm^{-1}). All spectra were baseline corrected and normalized to 2100 cm^{-1}.

2.7. UV Absorbance of Exposed Surfaces

UV–Vis absorption spectra of wood surfaces treated with NPs and untreated controls were collected over a wavelength range of 200–1100 nm using a spectrophotometer (Evolution 260, Thermo Fischer, Waltham, MA, USA) equipped with a diffuse reflectance accessory for solids. Diffuse reflectance (DR) of the samples was measured at a bandwidth of 2 nm, integration time of 0.15 s, and scan speed of 400 nm min^{-1}. After measurements, the data were normalized in order to establish a valid comparison. All measurements were performed in triplicate after 2880 min of UV (340 nm) irradiation.

2.8. Transmission Electron Microscopy and Scanning Electron Microscopy

TiO_2 and ZnO NPs were examined using transmission electron microscopy (TEM) prior to their use. TEM observations at 4 Å resolution were made in a JEOL-JEM transmission electron microscope (1200EX-II, Tokyo, Japan). The presence and distribution of NPs on wood surfaces after UV exposure were examined by scanning electron microscopy (SEM) with energy dispersive spectroscopy (EDS) analysis. Five by five mm^2 samples, cut from parent samples, were fixed with nylon nail polish to aluminum stubs. Fixed samples were stored over silica gel for 5 days and then coated with a gold layer (10 nm) with a sputter coater. SEM and EDS mapping images were obtained using a JSM scanning electron microscope (JSM-6380, Tokyo, Japan) at 20 kV accelerating voltage and 40 μm spot size.

2.9. X-ray Diffraction Analysis

After exposure, an X-ray diffraction analysis (XRD) was conducted on the samples to observe possible changes in their crystallographic configuration. A portion of each exposed surface was ground and sieved to 60 mesh and then analyzed in a D4-Endeavor X-ray diffraction analyzer (Bruker Optic Pvt. Ltd., Billerica, MA, USA) at λ = 0.154 nm, 2° s^{-1}, 300 rpm, and 2θ between 2° and 70°.

3. Results

The sizes and shapes of NPs, observed by TEM (Figure 1), are consistent with information provided by the manufacturer. The presence and distribution of NPs on wood surfaces after UV exposure were confirmed by SEM and EDS mapping analysis (Figure 2). Weight gain percentage in wooden samples ranged from 0.45 to 0.97% (rutile 50 nm and rutile 100 nm, respectively).

After UV (340 nm) exposure, the photocatalytic activity of TiO_2 and ZnO NPs was measured in vitro as intensity of ·OH radicals in arbitrary units (arb. Units) by using DMPO-OH adduct [32]. After 30 min of exposure (Figure 3), radical activity was undetectable in the presence of R50 (rutile 50 nm), R100 (rutile 100 nm), and A40 (anatase 40 nm), while the intensity was very small in the presence of A100 (anatase 100 nm). On the other hand, intensity was noticeable in the presence of ZnO (35 and 80), but ZnO80 produced the highest intensity for both ZnO NPs that were tested (near of 75% greater intensity). The entire data set for these results is shown in Figure S2 (Supplementary Data). These results show the photocatalytic effect of each type of nanoparticle with respect to its size. It can be seen that ZnOs are the most photoactive NPs, and larger-sized ones have a greater photocatalytic effect. On the other hand, none of the TiO_2 NPs exceeded the signal intensity of the DMPO-OH adduct, and only A100 was able to show a signal which was lower than both ZnO NPs.

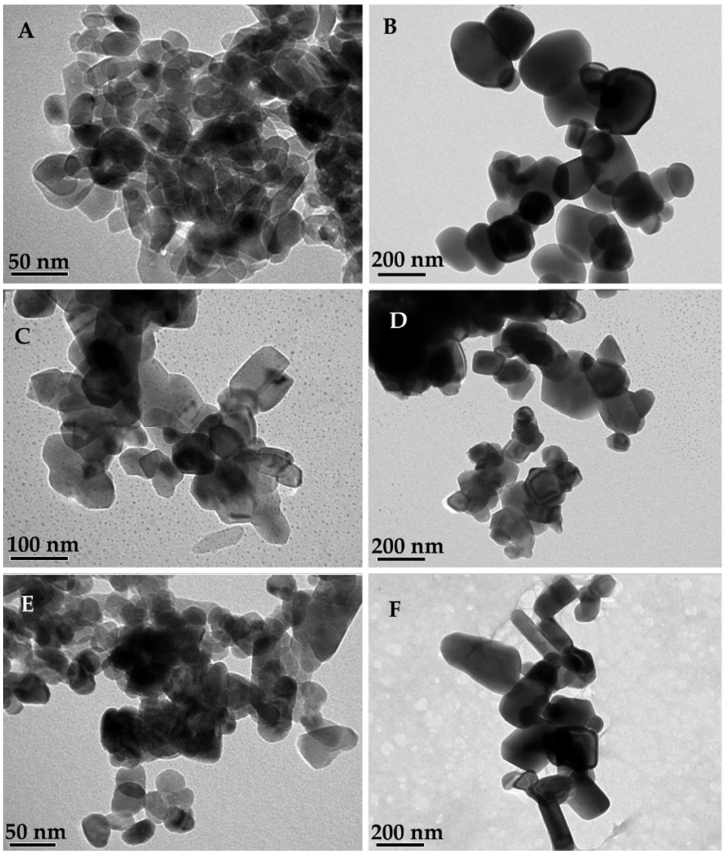

Figure 1. TEM images of (**A**) anatase 40 nm, (**B**) anatase 100 nm, (**C**) rutile 50 nm, (**D**) rutile 100 nm, (**E**) ZnO 35–45 nm, and (**F**) ZnO 80–200 nm.

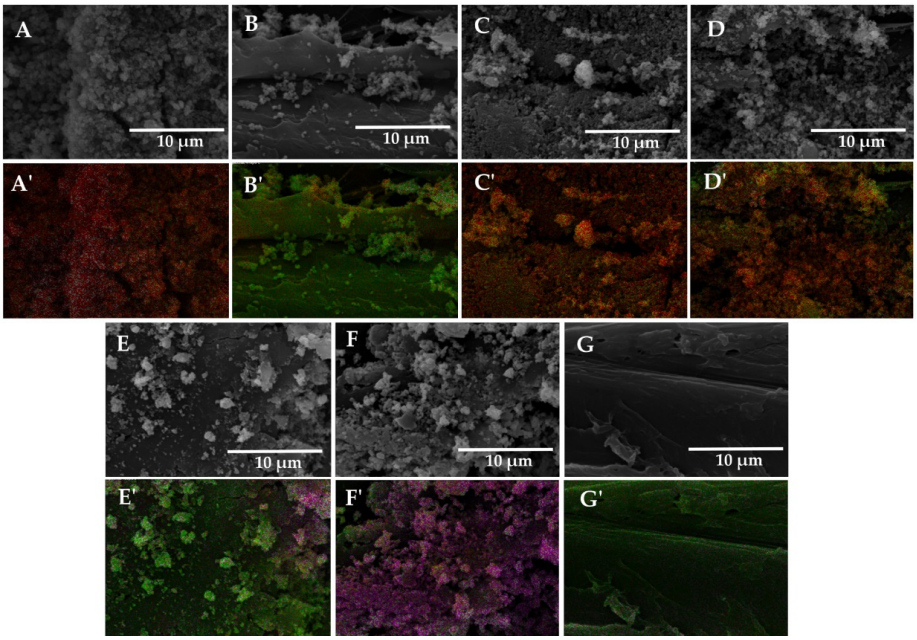

Figure 2. SEM images of wood surfaces treated with (**A**) anatase 40 nm, (**B**) anatase 100 nm, (**C**) rutile 50 nm, (**D**) rutile 100 nm, (**E**) ZnO 35–45 nm, and (**F**) ZnO 80–200 nm and (**G**) untreated control. EDS mapping images of wood surfaces treated with (**A′**) anatase 40 nm, (**B′**) anatase 100 nm, (**C′**) rutile 50 nm, (**D′**) rutile 100 nm, (**E′**) ZnO 35–45 nm, and (**F′**) ZnO 80–200 nm and (**G′**) untreated control, showing in red, purple, and green the distribution of Ti, Zn, and C, respectively. Images obtained after UV exposure.

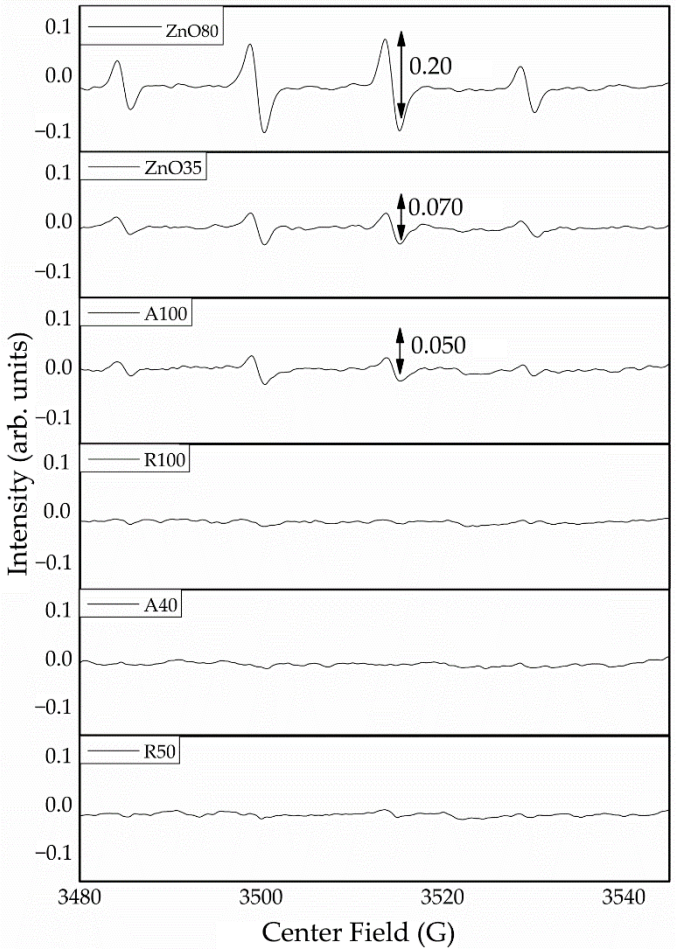

Figure 3. Intensity in arbitrary units (arb. units) of adducted hydroxyl radicals (·OH) produced by ZnO (ZnO 35−zinc oxide 35–45 nm and ZnO 80−zinc oxide 80–200 nm) and TiO_2 (A100−anatase 100 nm, A40−anatase 40 nm, R100−rutile 100 nm, and R50−rutile 50 nm) NPs following 30 min of irradiation, as measured using electron paramagnetic resonance (EPR) spectroscopy.

Radical activity on wood surfaces was measured on untreated and NP-treated surfaces, before and after UV exposure (Figure 4), in the EPR experiment that used smaller-sized radiata pine samples. On wood surfaces treated with the NPs, EPR tests revealed different signal intensities. This parameter is directly proportional to free radical concentration. In Figure 4, it can be observed that before UV exposure, radical activity was only detected in samples treated with ZnO NPs with no visible changes in color. This activation prior to irradiation may be due to the significant photoactivity of these NPs, possibly activated by ambient light in the laboratory. After 120 min of UV exposure, samples treated with ZnO35 showed the highest level of aromatic radical activity, followed by the untreated control, samples treated with A100, and then samples treated with ZnO80. Noticeably lower radical activity was detected for samples treated with R50 and R100, and even lower radical activity was found for samples treated with A40. After 1440 min of exposure, all samples showed increased intensities of phenoxy radicals. Trends observed initially, except for samples treated with ZnO NPs, were maintained. Samples treated with ZnO increased their level of aromatic radical activity, reaching the highest values of all samples. They were followed by control samples, then by samples treated with A100, R50, and R100. Again, the lowest intensity of radicals was observed for samples treated with A40. After 2880 min of UV exposure, the radical activity of samples treated with ZnO was still the highest among all samples, while the radical activity of all TiO_2-treated samples was distinctly lower than that of the untreated control samples. It is worth noting that after such UV irradiation

(2.65 W/m^2), radical activity of TiO_2 in rutile- and anatase-treated samples was similar in terms of intensity and behavior.

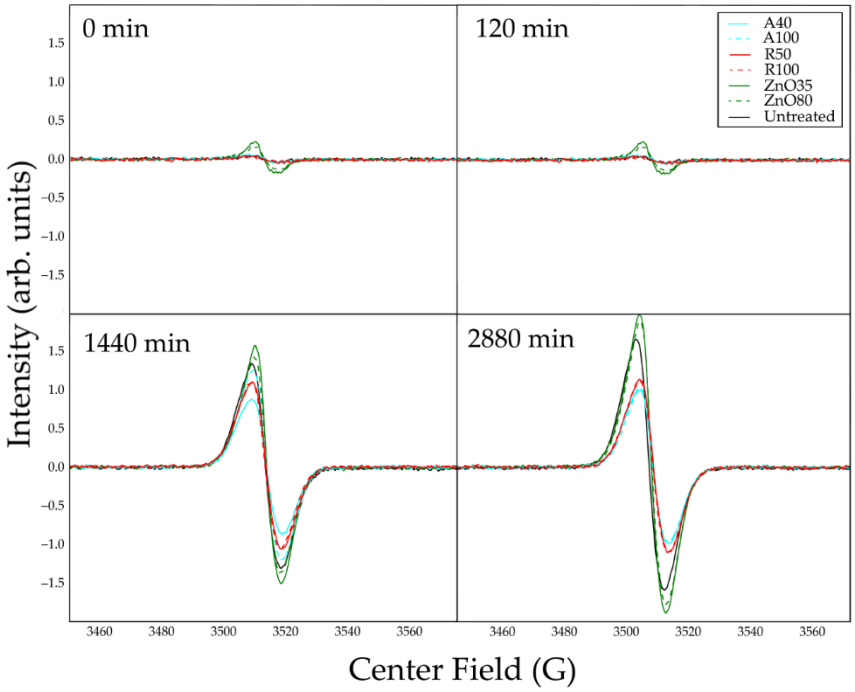

Figure 4. Radical activity in wood samples detected by electron paramagnetic resonance (EPR) for untreated control and samples treated with anatase 40 nm (A40), anatase 100 nm (A100), rutile 50 nm (R50), rutile 100 nm (R100), ZnO 35–45 nm (ZnO35), ZnO 80–200 nm (ZnO80), and untreated samples (control); before and after 120, 1440, and 2880 min of UV exposure (340 nm).

Chemical changes evaluated by FTIR-ATR at the surface of samples before and after exposure are shown in Figure 5. Untreated samples (control) showed noticeable changes in peaks at wavenumbers of 1600, 1508, and 1261 cm^{-1}, corresponding to C=C and C-O stretching in lignin [35,36]. These peaks decreased over time, indicating degradation of lignin with increasing exposure. Changes in peaks related to lignin were also observed in samples treated with NP, although depending on the treatment, photo-oxidative reactions occurred at different levels. Thus, changes in peaks at 1600, 1508, and 1261 cm^{-1} could be discerned in samples treated with R100 and ZnO80; changes in peaks at 1508 and 1261 cm^{-1} could be discerned in samples treated with ZnO35 and changes in peaks at 1600 and 1508 cm^{-1} could be discerned in samples treated with A100. All the above-mentioned samples also showed an increase in the peak at 1737 cm^{-1}, corresponding to the stretching of C=O groups and acetal groups in hemicelluloses [37], possibly due to the generation of carbonyl groups resulting from photo-oxidation. In contrast, samples treated with A40 nm were highly resistant to chemical changes due to UV radiation. Peaks at 1737, 1600, 1508, and 1261 cm^{-1} remained unchanged after 2880 min of exposure. FTIR-ATR measurement on samples treated with R50 showed no changes at peaks related to lignin after 120 min of UV irradiation. All attempts to obtain readings at these surfaces after 1440 and 2880 min of exposure were not successful.

After 2880 min of irradiation with UV (340 nm), a diffuse reflectance test was performed on wood samples to see changes in absorbances on wood surfaces. The test was carried out at wavelengths between 200–1100 nm. Similar profiles were obtained for all the samples. Figure 6 depicts the absorbance of wood surfaces between 300 and 500 nm. The full set of data is available in Figure S3 (Supplementary Data). In Figure 6, it is possible to observe the differences in the visible region of the spectrum. In the case of untreated wood (control), it showed a significant, and the largest, absorption band near 400 nm after UV irradiation. As described in the literature, this band is characteristic of the oxidation of

lignin-containing materials when irradiated with shortwave UV (λ < 385 nm) [38]. More specifically, the appearance of oxidized chromophore components of lignin is usually detected near this region at 400 nm [39]. Meanwhile, it was observed that for NP-treated samples, this absorption band decreased. However, ZnO35- and R100-treated samples still exhibited high absorbance in this region, but no new component developed. The opposite occurred with A40, so far the least photoactive NP, which showed the lowest absorbance in the 400 nm region. This indicates that when this NP is applied, fewer changes associated with the generation of chromophores on wood surfaces leading to color changes should be expected.

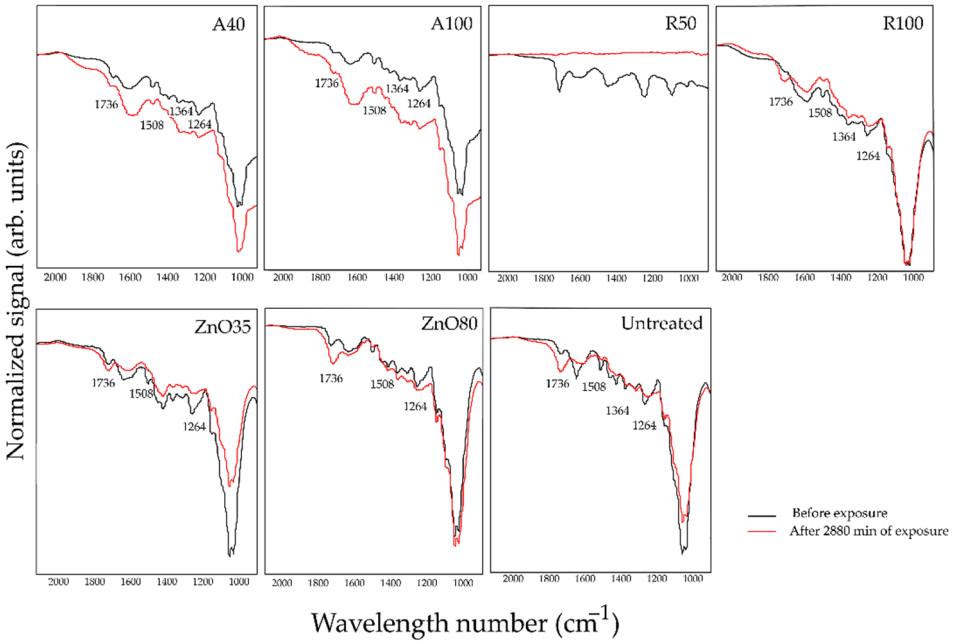

Figure 5. FTIR-ATR spectra of wood samples treated with anatase 40 nm (A40), anatase 100 nm (A100), rutile 50 nm (R50), rutile 100 nm (R100), ZnO 35–45 nm (ZnO35), ZnO 80–200 nm (ZnO80), and untreated samples (control); before and after 2880 min of UV exposure (340 nm), except R50, for whose spectra were obtained after 120 min of exposure.

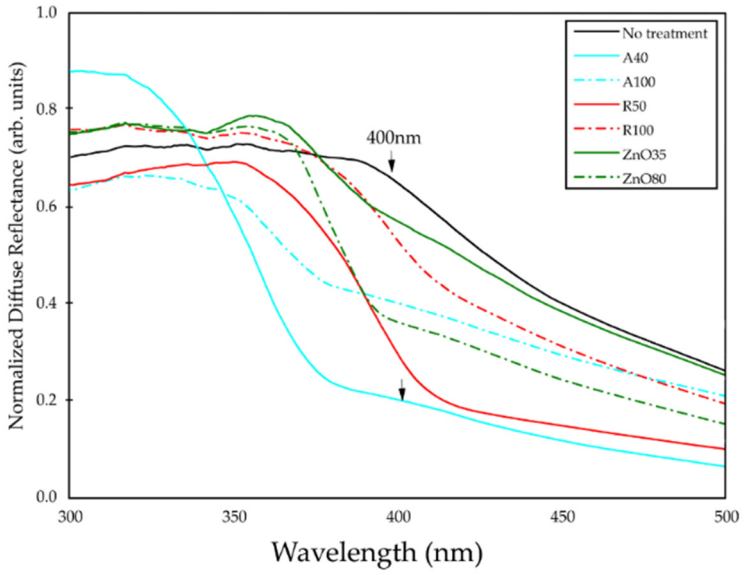

Figure 6. UV–Vis absorbance between 300–500 nm for untreated control and NP-treated samples.

Changes in color of irradiated wood surfaces expressed using the CIE L*a*b* system are shown in Figure 7. The ΔL* value (change in lightness) remained close to 0 from 0 to 2880 min, indicating that most color changes in samples were due to reddening and yellowing. The ΔL* in most samples treated with NPs increased initially, from 0 to 120 min, and then decreased from 120 to 2880 min. This trend was not observed in samples treated with ZnO80. In this case, ΔL* decreased throughout the exposure period, indicating darkening of the surface. The Δa* increased near 1 color unit for untreated control samples from 0 to 2880 min of exposure. Similar increases were also observed in samples treated with ZnO80 and R100. Less pronounced changes occurred in samples treated with ZnO35 and R50, and even smaller changes were detected in samples treated with A40 and A100. The Δb* values also increased in most samples over time. The highest increase, about 5 color units from 0 to 2880 min of exposure, occurred in untreated control samples, followed by R100, ZnO35, and then by Z80 and A100. A small increase in Δb* was observed in samples treated with R50. These samples showed an increase in their blueness–yellowness values from 120 to 1440 min, but after that Δb* remained constant during exposure. The opposite trend was observed for samples treated with A40, which in contrast to all other samples turned bluer rather the yellower during UV exposure. The macroscopic appearances of the treated and control samples are shown in Figure 8.

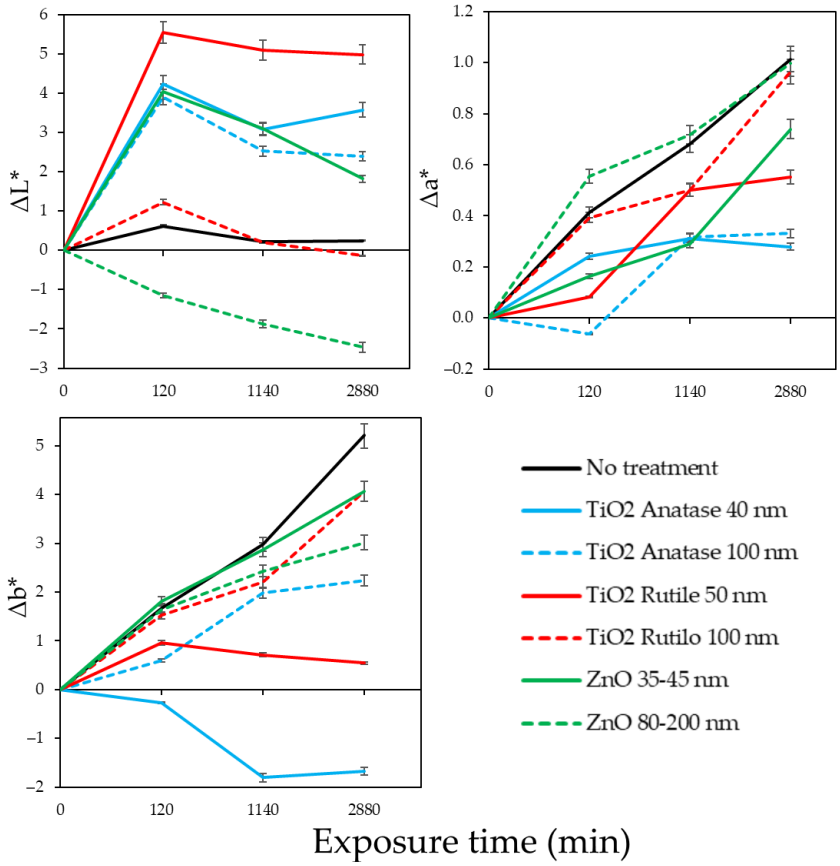

Figure 7. Changes in CIE L*a*b* color parameters ΔL*, Δa*, and Δb* of untreated control samples and samples treated with different NPs; before and after exposure to UV radiation at 340 nm. Bars represent 5% error.

Figure 9 shows the XRD patterns of wood samples treated with the nanoparticles after exposure. In all samples, peaks related to the diffraction angles of cellulose crystal planes (11.9°, 24.0°) can be observed [40]. In samples treated with TiO_2, no sharp peaks were found in samples treated with anatase, but changes in the curve can be discerned at diffraction angles 38°, 48°, and 54.7°, which correspond to crystalline anatase. Conversely, samples treated with rutile showed more defined peaks at the diffraction angles 27.4°, 36.1°,

41.3°, and 54.4°, which have been reported for crystalline rutile [41]. In samples treated with ZnO, several peaks described for wurtzite (31.11°, 34.13°, 35.56°, 47.03°, 56.01°, 62.12°, 67.29, and 68.28°) were observed [42]. These results suggest that no major changes in the crystallinity of the nanoparticles occurred due to UV exposure.

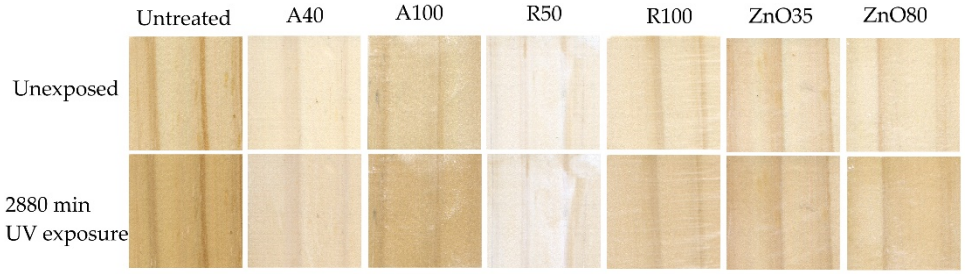

Figure 8. Appearance of wood samples treated with anatase 40 nm (A40), anatase 100 nm (A100), rutile 50 nm (R50), rutile 100 nm (R100), ZnO 35–45 nm (ZnO35), ZnO 80–200 nm (ZnO80), and untreated control samples before and after UV exposure.

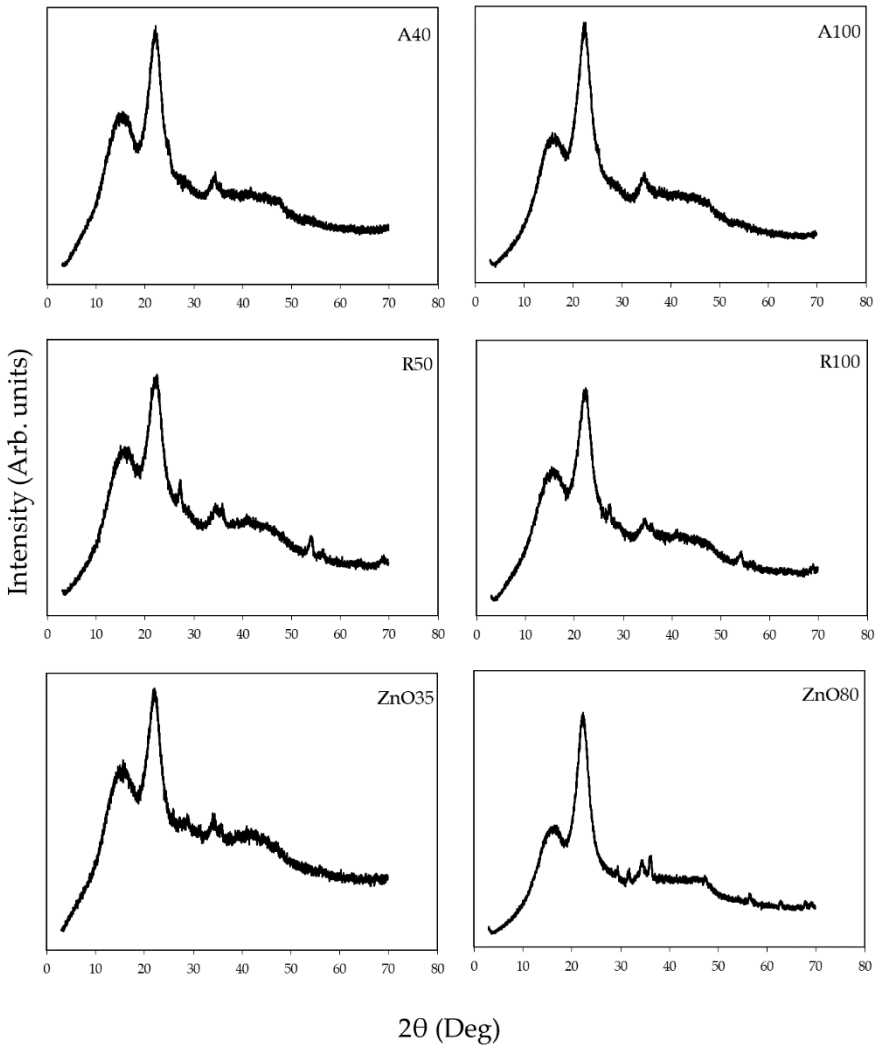

Figure 9. XRD patterns for wood samples treated with anatase 40 nm (A40), anatase 100 nm (A100), rutile 50 nm (R50), rutile 100 nm (R100), ZnO 35–45 nm (ZnO35), and ZnO 80–200 nm (ZnO80). All readings were performed after UV exposure.

4. Discussion

During exposure to UV and visible light, the chemical components of wood absorb radiation at different wavelengths, and photodegradation of wood occurs [3]. In the presence of NPs, absorption of radiation can be altered by reflection and scattering, but photodegradation is also affected by the photocatalytic properties of NPs [43]. Hence, the combination of these effects will alter the outcome of UV exposure. In our experiment, the results of UV exposure differed according to the NPs used to treat wood. Thus, after UV irradiation, the organic radical production, typically phenoxy radicals, was the highest on wood surfaces treated with ZnO, followed by untreated surfaces, and then by surfaces treated with TiO_2. In conditions of direct exposure, TiO_2 nanoparticles appear more stable than ZnO in terms of photocatalytic activity [44,45]. The higher intensity of phenoxy radicals detected by EPR in wood samples treated with ZnO in comparison with that of samples treated with TiO_2 hints at the possible contribution of the radical species produced by the photosensitizer to the photodegradation of wood.

Several photochemical routes to phenoxyl radicals have been proposed, however, the formation and reactivity of phenoxyl radicals in the lignin matrix is not well understood. Several photochemical studies using model compounds in solution or adsorbed on solid supports have provided some insights into the factors influencing the proposed pathways. Direct irradiation studies on lignin model compounds have provided evidence for the involvement of hydrogen abstraction reactions from phenols, β-cleavage of substituted a-aryloxyacetophenones, and the cleavage of ketyl radicals formed by photoreduction in aromatic ketones or hydrogen abstraction from arylglycerol β-aryl ethers in the photo-yellowing of lignin [38,46,47]. A summary of the main reaction pathways that were identified for the photo-yellowing of wood surfaces is shown in Figure S4 (Supplementary Material) [48–50]. Only the β-aryl ethers (β-O-4 linkages) were considered, because they are the most abundant linkages in lignin of hardwood and softwood (>45%) [46].

The literature suggests that one way to follow the photo-oxidation of wood is to study the yellowing produced at irradiated wood surfaces [3]. This approach can follow three main pathways: (1) absorption of UV/VIS radiation by photoactive groups in lignin; (2) formation of intermediates (mainly radicals); and (3) formation of chromophores. Notwithstanding, other pathways that do not include phenoxy radicals may also be involved in the photodegradation of lignin and resulting color changes. For example, previous reports have stated that oxygen (O_2), in particular singlet oxygen ($^1O_2$), is involved in the photodegradation of wood, producing phenoxy radicals and hydroperoxides [51–53]. Radical activity in wood samples exposed to UV radiation has been mainly attributed to phenoxy/semiquinone radicals generated from the photolysis of lignin [49,54–56]. Phenoxy radicals are readily produced from phenolic hydroxy groups by the action of light. Other species, such as peroxy-radicals are typically short-lived due to their chemical reactivity, and therefore might be not accumulated at detectable concentrations by EPR [52].

The experimental results show that the ZnO NP produced the highest intensity of ·OH species in vitro. These radicals in excess may also interact with the substrate, enhancing lignin depolymerization, leading to color changes, and even driving the microbial degradation of wood [51,57,58]. These results agree with previous reports that indicate that an excess of ·OH radicals on aromatic substrates leads to the formation of hydroxycyclohexadienyl radicals that subsequently lead to phenoxy radicals [52,55]. Thus, there is a relationship between the photoactivity of the NP to produce ·OH radicals with the increased degradation of lignin on the surface of wood.

The EPR signal shown in Figure 4 indicates strong formation of further C-centered semiquinone radicals generated through photolysis of wood treated with ZnO NP. The lifetimes of these radicals extended well beyond the illumination period [55]. In presence of TiO_2 NPs, the oxidation of lignin compounds was considerably lower, particularly on surfaces treated with smaller-sized NPs, in accord with the ability of TiO_2 in its rutile and anatase forms to photostabilize wood surfaces. However, the fact that the intensity of phenoxy radicals at all surfaces treated with TiO_2 NPs was practically the same after

2880 min of exposure indicates that at such a point, photochemical reactions were well advanced and, possibly, the surfaces were near to their chemical equilibrium. According to Feist and Hon 1984 [1], photodegradative reaction occurs at early stages of UV irradiation with the accumulation of resultant products on wood surfaces. During natural exposure to solar radiation, these products are removed by rain or become a carbon source for microorganisms [53].

At early stages of UV exposure, after 120 and 1440 min, it was observed that the intensity of phenoxy radicals on surfaces treated with anatase 100 nm was equal to that of untreated control samples, while surfaces treated with anatase 40 nm always showed a lower intensity. The chemical analysis of irradiated surfaces revealed that chemical changes were more evident in surfaces treated with 100 nm anatase and almost absent in surfaces containing 40 nm anatase. In addition, under in vitro conditions, 40 nm anatase did not show photocatalytic activity, while 100 nm anatase produced the highest intensity of ·OH radicals of all TiO_2 NPs tested. The higher photoactivity of anatase 100 nm, shown in vitro, might explain the organic radicals present on wood surfaces treated with this NP during the early stages of UV irradiation. Therefore, it seems that the absence of photocatalytic activity under UV excitation, in addition to reflection and scattering, might be responsible for the photoprotective effect of anatase 40 nm observed here.

No differences in the production of organic radicals were detected between the surfaces treated with the two types of rutile NPs. Moreover, surfaces treated with rutile NPs always showed an intensity of organic radicals lower than that of surfaces treated with ZnO, irrespective of exposure times. In addition, surfaces treated with rutile NPs showed fewer organic radicals than surfaces treated with 100 nm anatase but higher than those of surfaces treated with 40 nm anatase both after 120 and 1440 min of UV exposure. As indicated above, after 2880 min of exposure, all TiO_2 NP-treated samples showed similar intensities of organic radicals. Despite these similarities, color changes, UV–Vis light absorbance profiles, and chemical changes show that rutile 50 nm was more efficient at preventing photodegradation than rutile 100 nm. It can be inferred that rutile 50 nm was more efficient at blocking and scattering UV radiation, or was able to act as an electron sink to neutralize the effect of organic radicals, as proposed by Hernandez et al. in 2020 [30].

Several differences between anatase and rutile are described at a functional level. For instance, anatase has higher absorbance affinity for organic compounds than rutile and a lower recombination rate [59]. Similarly, due to band-gap differences, anatase is prone to absorb radiation in the UV range, while the excitation wavelength for rutile can extend into the visible spectrum. Hence, anatase is regarded as more photochemically active due to the effect of lower recombination rates and higher surface adsorptive capacity and, in mixtures of anatase–rutile, anatase is considered the active component, while rutile takes a passive role, acting as an electron sink [60]. In our experiment, differences in the level of photoactivity of anatase and rutile upon excitation with UV light at 340 nm seemed more related to their size than to their crystallographic configuration.

Several studies have addressed the problem of photodegradation of wood surfaces due to UV radiation by treating wood with nanoparticles. These studies normally examine the use of NPs as components of coatings or explore novel methods to deposit NPs on wood surfaces, avoiding agglomerations and discontinuous layers. Direct treatment of wood surfaces with NPs is not very common, mainly due to potential leaching of the NPs when wood is exposed to moisture. However, Nair et al. (2018) [61] studied the photostabilization of *Wrightia tinctoria* (Pala Indigo) with different concentrations of ZnO 65–90 nm, TiO_2 26–38 nm, and CeO_2 15–25 nm nanoparticles, which were applied onto surfaces in propylene glycol suspensions and thereafter extensively irradiated with artificial UV radiation at 340 nm. Our results confirm the trends observed by these authors. In their study, all treatments successfully decreased wood photodegradation, with a clear influence of the initial concentration of the nanoparticles applied and resulting photoprotective effects. The greater ability of TiO_2 to suppress photodegradation, color, and chemical changes compared with ZnO was observed, and the darkening of surfaces treated with ZnO and bluer

surfaces after UV exposure in samples treated with TiO_2 were also noted. Unfortunately, no information on the level of photoactivity of the nanoparticles was reported by the authors.

The physiochemical properties of TiO_2 and ZnO are relevant to the ability of NP compounds (semiconductors) to attenuate UV radiation [62,63]. For instance, the refractive indexes of anatase and rutile, when forming polycrystalline films, have been reported as 3.6 and 4.0, respectively [64], while in wurtzite, the most common state of ZnO, the refractive indexes lies between 2.0 and 2.3 [65]. These differences explain why TiO_2 produces a whitening of surfaces, while ZnO is essentially transparent [43]. This supports the observations made on the lightness change results, which indicate that most samples treated with NPs became lighter than untreated controls upon UV exposure, except those treated with rutile 100 nm, which followed a lightness pattern similar to untreated controls, and samples treated with ZnO 80–200 nm, which became darker than controls, possibly due to the transparency of this NP. The band-gap energy for bulk anatase, rutile, and wurtzite have been reported as 3.03, 3.20 eV, and 3.37 eV, respectively, at room temperature [64,66,67]. Consequently, it has been stated that TiO_2 absorbs preferentially in the UV range while scattering and reflecting visible light. However, the valence band of TiO_2 is densely packed with electron states, allowing many absorption possibilities. Therefore, TiO_2 absorbs more in the UVB range, while ZnO absorbs more UVA, although the band-gap energy of TiO_2 is lower than that of ZnO [67]. Smilj and Pavel (2011) [43] have pointed out that not only size-related optical particle properties can influence the ability of TiO_2 and ZnO to attenuate UV radiation but also the surrounding media. In this case, the deposition of NPs on wood surfaces, and the agglomeration of NPs, could have affected the photoprotective properties of the different NPs. In the same way, agglomeration could have affected the measurement of photocatalytic activity in vitro, as smaller-sized NPs are expected to be more photoactive due to their increased specific surface area [68]. This unexpected outcome requires further research to be clarified.

In our previous work, based on the suppression of photocatalytic activity of rutile NPs, we theorized that certain levels of photoactivity may make a positive contribution to decreasing the photodegradation of wood surfaces via an electron sink mechanism [30]. In this work, our observations indicate that this is unlikely to occur in highly photoactive NPs, such as ZnO of sizes 35–45 nm and 80–200 nm. Apparently, the excess of ·OH species may favor the development of phenoxy radicals, leading to chemical and color changes on wood surfaces. Thus, despite the transparency of ZnO, at nanoscale, this photosensitizer is less effective than TiO_2 at attenuating the effects of UV radiation on wood surfaces. The size of the NP also appeared as a relevant factor, where smaller-sized NPs were the most effective at preventing photochemical reactions, while being less photoactive in vitro. The crystallographic configuration of the different TiO_2 NPs tested does not seem to be so relevant during longer-term exposure of treated surfaces to UV radiation.

In this study, the resources and the difficulties associated with the EPR readings on wood surfaces limited the number of tested replicates. Therefore, in future research, it may be appropriate to confirm the tendencies observed in the results section but also to explore the effects of other factors that induce or accelerate photodegradation on wood surfaces.

5. Conclusions

We measured the photoactivity of ZnO and TiO_2 NPs of different type, size, and crystallographic configuration in vitro and examined the ability of these NPs to photostabilize radiata pine wood samples exposed to 340 nm UV radiation. The experimental results show that highly photocatalytic NPs enhance chemical changes due to photodegradation, while less photoactive NPs are better at reducing chemical and color changes upon UV irradiation. Thus, less photoactive TiO_2 NPs were better on wood photo protection than highly photoactive ZnO NPs. Similarly, smaller-sized NPs showed greater ability to reduce photochemical reactions than larger-sized NPs. Hence, we conclude that in vitro measurements of photocatalytic properties of NPs provide a useful guide to their short-term performance as photostabilizers for wood. For long-term exposure difference between

TiO_2 NPs, anatase and rutile appeared less relevant. In a previous study, we observed that certain levels of photoactivity in TiO_2 NPs may make a positive contribution to decreasing the photodegradation of wood surfaces by an electron sink mechanism. In this work, our observations indicate that this is unlikely to occur in the presence of highly photoactive NPs.

Supplementary Materials: The following supporting information can be downloaded at: https://www.mdpi.com/article/10.3390/f13111922/s1, Figure S1: SEM image showing nanoparticles inside wood after vacuum-assisted impregnation. Figure S2: Intensity of ·OH radicals in arbitrary units by using DMPO-OH adduct. Figure S3: UV–Vis absorbance between 200–1100 nm of untreated control and NP-treated samples. Figure S4: Summary of the main pathways reported in the formation of phenoxy radicals in lignin.

Author Contributions: Conceptualization, V.A.H., R.R. and P.D.E.; methodology, V.A.H., R.R. and N.S.; formal analysis, V.A.H., R.R. and D.C.; writing—original draft preparation, V.A.H. and R.R.; writing—review and editing, V.A.H., D.C., R.R. and P.D.E.; supervision, V.A.H., D.C. and P.D.E. All authors have read and agreed to the published version of the manuscript.

Funding: This research was funded by ANID, Fondecyt 11180030, and NSERC Discovery 327380-2013.

Institutional Review Board Statement: Not applicable.

Informed Consent Statement: Not applicable.

Data Availability Statement: Not applicable.

Acknowledgments: V.H. acknowledges the support from PAI Convocatoria Nacional Subvención a Instalación en la Academia 2018, 77180054. D.C. and R.R. thanks the support from FONDAP Solar Energy Research Center ANID/FONDAP/15110019.

Conflicts of Interest: The authors declare no conflict of interest. The funder had no role in the design of the study; in the collection, analyses, or interpretation of data; in the writing of the manuscript, or in the decision to publish the results.

References

1. Feist, W.C.; Hon, D.N.S. Chemistry of Weathering and Protection. In *The Chemistry of Solid Wood*; American Chemical Society: Washington, DC, USA, 1984; pp. 401–451.
2. George, B.; Suttie, E.; Merlin, A.; Deglise, X. Photodegradation and Photostabilisation of Wood–the State of the Art. *Polym. Degrad. Stab.* **2005**, *88*, 268–274. [CrossRef]
3. Evans, P.D. Weathering and Photoprotection of Wood. In *Development of Commercial Wood Preservatives*; ACS Symposium Series; American Chemical Society: Washington, DC, USA, 2008; Volume 982, pp. 69–117.
4. Derbyshire, H.; Miller, E.R. The Photodegradation of Wood during Solar Irradiation. *Holz Als Roh- Und Werkstoff* **1981**, *39*, 341–350. [CrossRef]
5. Diffey, B.L. Solar Ultraviolet Radiation Effects on Biological Systems. *Phys. Med. Biol.* **1991**, *36*, 299–328. [CrossRef] [PubMed]
6. Evans, P.D.; Haase, J.G.; Seman, A.; Kiguchi, M. The Search for Durable Exterior Clear Coatings for Wood. *Coatings* **2015**, *5*, 830–864. [CrossRef]
7. Jirouš-Rajković, V.; Miklečić, J. Enhancing Weathering Resistance of Wood—A Review. *Polymers* **2021**, *13*, 1980. [CrossRef]
8. Petrič, M. Surface Modification of Wood: A Critical Review. *Rev. Adh. Adhes.* **2013**, *1*, 216–247. [CrossRef]
9. Williams, R.S.; Feist, W.C. Wood Modified by Inorganic Salts: Mechanism and Properties. I. Weathering Rate, Water Repellency, and Dimensional Stability of Wood Modified with Chromium (III) Nitrate versus Chromic Acid. *Wood Fiber Sci.* **1985**, *17*, 184–198.
10. Deka, M.; Humar, M.; Rep, G.; Kričej, B.; Šentjurc, M.; Petrič, M. Effects of UV Light Irradiation on Colour Stability of Thermally Modified, Copper Ethanolamine Treated and Non-Modified Wood: EPR and DRIFT Spectroscopic Studies. *Wood Sci. Technol.* **2008**, *42*, 5–20. [CrossRef]
11. Zhu, Y.; Evans, P.D. Surface Protection of Wood with Metal Acetylacetonates. *Coatings* **2021**, *11*, 916. [CrossRef]
12. Schaller, C.; Rogez, D. New Approaches in Wood Coating Stabilization. *J. Coat. Technol. Res.* **2007**, *4*, 401–409. [CrossRef]
13. Evans, P.D.; Chowdhury, M. Photoprotection of Wood Using Polyester-Type UV-Absorbers Derived from the Reaction of 2-Hydroxy-4(2,3-Epoxypropoxy)-Benzophenone with Dicarboxylic Acid Anhydrides. *J. Wood Chem. Technol.* **2010**, *30*, 186–204. [CrossRef]
14. Schauwecker, C.F.; McDonald, A.G.; Preston, A.F.; Morrell, J.J. Use of Iron Oxides to Influence the Weathering Characteristics of Wood Surfaces: A Systematic Survey of Particle Size, Crystal Shape and Concentration. *Eur. J. Wood Prod.* **2014**, *72*, 669–680. [CrossRef]

15. Blackburn, S.R.; Meldrum, B.J.; Clayton, J. The Use of Fine Particle Titanium Dioxide for UV Protection in Wood Finishes. *Faerg Och Lack Scand.* **1991**, *37*, 192–196.
16. Zanatta, P.; Lazarotto, M.; Gonzalez de Cademartori, P.; Cava, S.; Moreira, M.; Gatto, D. The Effect of Titanium Dioxide Nanoparticles Obtained by Microwave-Assisted Hydrothermal Method on the Color and Decay Resistance of Pinewood. *Maderas Cienc. Tecnol.* **2017**, *19*, 495–506. [CrossRef]
17. Fufa, S.M.; Jelle, B.P.; Hovde, P.J. Effects of TiO_2 and Clay Nanoparticles Loading on Weathering Performance of Coated Wood. *Prog. Org. Coat.* **2013**, *76*, 1425–1429. [CrossRef]
18. Egerton, T.A. UV-Absorption—The Primary Process in Photocatalysis and Some Practical Consequences. *Molecules* **2014**, *19*, 18192–18214. [CrossRef] [PubMed]
19. Beydoun, D.; Amal, R.; Low, G.; McEvoy, S. Role of Nanoparticles in Photocatalysis. *J. Nanopart. Res.* **1999**, *1*, 439–458. [CrossRef]
20. Brezová, V.; Gabčová, S.; Dvoranová, D.; Staško, A. Reactive Oxygen Species Produced upon Photoexcitation of Sunscreens Containing Titanium Dioxide (an EPR Study). *J. Photochem. Photobiol. B Biol.* **2005**, *79*, 121–134. [CrossRef]
21. Gladis, F.; Schumann, R. A Suggested Standardised Method for Testing Photocatalytic Inactivation of Aeroterrestrial Algal Growth on TiO_2-Coated Glass. *Int. Biodeterior. Biodegrad.* **2011**, *65*, 415–422. [CrossRef]
22. Jain, A.; Vaya, D.; Jain, A.; Vaya, D. Photocatalytic Activity of TiO_2 Nanomaterials. *J. Chil. Chem. Soc.* **2017**, *62*, 3683–3690. [CrossRef]
23. Nevárez-Martínez, M.; Espinoza-Montero, P.; Quiroz-Chávez, F.; Ohtani, B. Fotocatálisis: Inicio, actualidad y perspectivas a través del TiO_2. *Av. En Quim.* **2017**, *12*, 45–59.
24. Hughes, W. *Photodegradation of Paint Films Containing TiO_2 Pigments*; Verlag Chemie GmbH: Weinheim/Bergst, Germany, 1970; pp. 67–82.
25. Allen, N.S.; McKellar, J.F.; Phillips, G.O.; Chapman, C.B. The TiO_2 Photosensitized Degradation of Nylon 6, 6: Stabilizing Action of Manganese Ions. *J. Polym. Sci. Polym. Lett. Ed.* **1974**, *12*, 723–727. [CrossRef]
26. Tsuzuki, T.; He, R.; Wang, J.; Sun, L.; Wang, X.; Hocking, R. Reduction of the Photocatalytic Activity of ZnO Nanoparticles for UV Protection Applications. *Int. J. Nanotechnol.* **2012**, *9*, 1017–1029. [CrossRef]
27. Xiao, L.; Youji, L.; Feitai, C.; Peng, X.; Ming, L. Facile Synthesis of Mesoporous Titanium Dioxide Doped by Ag-Coated Graphene with Enhanced Visible-Light Photocatalytic Performance for Methylene Blue Degradation. *RSC Adv.* **2017**, *7*, 25314–25324. [CrossRef]
28. Gu, Y.; Guo, B.; Yi, Z.; Wu, X.; Zhang, J.; Yang, H. Morphology Modulation of Hollow-Shell ZnSn(OH)6 for Enhanced Photodegradation of Methylene Blue. *Colloids Surf. A Physicochem. Eng. Asp.* **2022**, *653*, 129908. [CrossRef]
29. Li, Y.; Li, M.; Xu, P.; Tang, S.; Liu, C. Efficient Photocatalytic Degradation of Acid Orange 7 over N-Doped Ordered Mesoporous Titania on Carbon Fibers under Visible-Light Irradiation Based on Three Synergistic Effects. *Appl. Catal. A Gen.* **2016**, *524*, 163–172. [CrossRef]
30. Hernandez, V.A.; Morales, C.; Sagredo, N.; Perez-Gonzalez, G.; Romero, R.; Contreras, D. Radical Species Production and Color Change Behavior of Wood Surfaces Treated with Suppressed Photoactivity and Photoactive TiO_2 Nanoparticles. *Coatings* **2020**, *10*, 1033. [CrossRef]
31. Numano, T.; Xu, J.; Futakuchi, M.; Fukamachi, K.; Alexander, D.B.; Furukawa, F.; Kanno, J.; Hirose, A.; Tsuda, H.; Suzui, M. Comparative Study of Toxic Effects of Anatase and Rutile Type Nanosized Titanium Dioxide Particles in Vivo and in Vitro. *Asian Pac. J. Cancer Prev.* **2014**, *15*, 929–935. [CrossRef]
32. Yamazaki, I.; Piette, L.H. ESR Spin-Trapping Studies on the Reaction of Fe^{2+} Ions with H_2O_2-Reactive Species in Oxygen Toxicity in Biology. *J. Biol. Chem.* **1990**, *265*, 13589–13594. [CrossRef]
33. Hernandez, V.A.; Evans, P.D. Technical Note: Melanization of the Wood-Staining Fungus *Aureobasidium pullulans* in Response to UV Radiation. *Wood Fiber Sci.* **2015**, *47*, 1–5.
34. Kropat, M.; Hubbe, M.A.; Laleicke, F. Natural, Accelerated, and Simulated Weathering of Wood: A Review. *Bioresources* **2020**, *15*, 9998–10062. [CrossRef]
35. Faix, O. Classification of Lignins from Different Botanical Origins by FT-IR Spectroscopy. *Holzforschung* **1991**, *45*, 21–28. [CrossRef]
36. Harrington, K.J.; Higgins, H.G.; Michell, A.J. Infrared Spectra of *Eucalyptus regnans* F. Muell and Pinus Radiata D. Don. *Holzforschung* **1964**, *18*, 108–113. [CrossRef]
37. Lionetto, F.; Del Sole, R.; Cannoletta, D.; Vasapollo, G.; Maffezzoli, A. Monitoring Wood Degradation during Weathering by Cellulose Crystallinity. *Materials* **2012**, *5*, 1910–1922. [CrossRef]
38. Paulsson, M.; Parkas, J. Review: Light-Induced Yellowing of Lignocellulosic Pulps–Mechanisms and Preventive Methods. *Bioresources* **2012**, *7*, 5995–6040. [CrossRef]
39. Gratzl, J. Lichtinduzierte Vergilbung von Zellstoffen: Ursachen Und Verhütung. *Papier* **1985**, *39*, 14–23.
40. Dong, Y.; Yan, Y.; Wang, K.; Li, J.; Zhang, S.; Xia, C.; Shi, S.Q.; Cai, L. Improvement of Water Resistance, Dimensional Stability, and Mechanical Properties of Poplar Wood by Rosin Impregnation. *Eur. J. Wood Prod.* **2016**, *74*, 177–184. [CrossRef]
41. Wang, J.; Yu, J.; Zhu, X.; Kong, X.-Z. Preparation of Hollow TiO_2 Nanoparticles through TiO_2 Deposition on Polystyrene Latex Particles and Characterizations of Their Structure and Photocatalytic Activity. *Nanoscale Res. Lett.* **2012**, *7*, 646. [CrossRef]
42. Khan, Y.A.; Singh, B.J.; Ullah, R.; Shoeb, M.; Naqvi, A.H.; Abidi, S.M.A. Anthelmintic Effect of Biocompatible Zinc Oxide Nanoparticles (ZnO NPs) on *Gigantocotyle explanatum*, a Neglected Parasite of Indian Water Buffalo. *PLoS ONE* **2015**, *10*, e0133086. [CrossRef]

43. Smijs, T.G.; Pavel, S. Titanium Dioxide and Zinc Oxide Nanoparticles in Sunscreens: Focus on Their Safety and Effectiveness. *Nanotechnol. Sci. Appl.* **2011**, *4*, 95–112. [CrossRef]
44. Bennett, S.W.; Keller, A.A. Comparative Photoactivity of CeO_2, γ-Fe_2O_3, TiO_2 and ZnO in Various Aqueous Systems. *Appl. Catal. B* **2011**, *102*, 600–607. [CrossRef]
45. Lewicka, Z.A.; Colvin, V.L. Photoactivity Tests of TiO_2 and ZnO Sunscreen Ingredients. *MRS Online Proc. Libr.* **2012**, *1413*, 1–6. [CrossRef]
46. Lanzalunga, O.; Bietti, M. Photo- and Radiation Chemical Induced Degradation of Lignin Model Compounds. *J. Photochem. Photobiol. B Biol.* **2000**, *56*, 85–108. [CrossRef]
47. Fabbri, C.; Bietti, M.; Lanzalunga, O. Generation and Reactivity of Ketyl Radicals with Lignin Related Structures. On the Importance of the Ketyl Pathway in the Photoyellowing of Lignin Containing Pulps and Papers. *J. Org. Chem.* **2005**, *70*, 2720–2728. [CrossRef]
48. Williams, R.S. Weathering of Wood. In *Handbook of Chemistry and Wood Composites*; CRC Press: Boca Raton, FL, USA, 2005; pp. 139–185.
49. Hon, D.N.S. Photochemical Degradation of Lignocellulosic Materials. In *Developments in Polymer Degradation–3*; Essex: Applied Science Ltd.: London, UK, 1981; pp. 229–281.
50. Huang, Y.; Pagé, D.; Wayner, D.D.; Mulder, P. Radical-Induced Degradation of a Lignin Model Compound. Decomposition of 1-Phenyl-2-Phenoxyethanol. *Can. J. Chem.* **1995**, *73*, 2079–2085. [CrossRef]
51. Hon, D.N.S.; Chang, S.T.; Feist, W.C. Participation of Singlet Oxygen in the Photodegradation of Wood Surfaces. *Wood Sci. Technol.* **1982**, *16*, 193–201. [CrossRef]
52. Hon, D.N.S.; Feist, W.C. Hydroperoxidation in Photoirradiated Wood Surfaces. *Wood Fiber Sci.* **1992**, *24*, 448–455.
53. Evans, P.D. Weathering of Wood and Wood Composites. In *Handbook of Wood Chemistry and Wood Composites*; CRC Press: Boca Raton, FL, USA, 2013; pp. 151–200.
54. Hon, D.N.S.; Ifju, G.; Feist, W.C. Characteristics of Free Radicals in Wood. *Wood Fiber* **1980**, *12*, 121–130.
55. Baur, S.I.; Easteal, A.J. ESR Studies on the Free Radical Generation in Wood by Irradiation with Selected Sources from UV to IR Wavelength Regions. *Holzforschung* **2014**, *68*, 775–780. [CrossRef]
56. Hon, D.N.S.; Ifju, G. Measuring Penetration of Light into Wood by Detection of Photo-Induced Free Radicals. *Wood Sci.* **1978**, *11*, 118–127.
57. Backa, S.; Gierer, J.; Reitberger, T.; Nilsson, T. Hydroxyl Radical Activity in Brown-Rot Fungi Studied by a New Chemiluminescence Method. *Holzforschung* **1992**, *46*, 61–67. [CrossRef]
58. Tanaka, H.; Itakura, S.; Enoki, A. Hydroxyl Radical Generation by an Extracellular Low-Molecular-Weight Substance and Phenol Oxidase Activity during Wood Degradation by the White-Rot Basidiomycete *Trametes versicolor*. *J. Biotechnol.* **1999**, *75*, 57–70. [CrossRef]
59. Stafford, U.; Gray, K.A.; Kamat, P.V.; Varma, A. An in Situ Diffuse Reflectance FTIR Investigation of Photocatalytic Degradation of 4-Chlorophenol on a TiO_2 Powder Surface. *Chem. Phys. Lett.* **1993**, *205*, 55–61. [CrossRef]
60. Hurum, D.C.; Agrios, A.G.; Gray, K.A.; Rajh, T.; Thurnauer, M. Explaining the Enhanced Photocatalytic Activity of Degussa P25 Mixed-Phase TiO_2 Using EPR. *J. Phys. Chem. B* **2003**, *107*, 4545–4549. [CrossRef]
61. Nair, S.; Nagarajappa, G.S.; Pandey, K.K. UV Stabilization of Wood by Nano Metal Oxides Dispersed in Propylene Glycol. *J. Photochem. Photobiol. B Biol.* **2018**, *183*, 1–10. [CrossRef] [PubMed]
62. Takahashi, K.; Yoshikawa, A.; Sandhu, A. *Wide Bandgap Semiconductors: Fundamental Properties and Modern Photonic and Electronic Devices*; Springer Science & Business Media: Berlin/Heidelberg, Germany, 2007; ISBN 978-3-540-47235-3.
63. Umebayashi, T.; Yamaki, T.; Itoh, H.; Asai, K. Analysis of Electronic Structures of 3d Transition Metal-Doped TiO_2 Based on Band Calculations. *J. Phys. Chem. Solids* **2002**, *63*, 1909–1920. [CrossRef]
64. Tanemura, S.; Miao, L.; Wunderlich, W.; Tanemura, M.; Mori, Y.; Toh, S.; Kaneko, K. Fabrication and Characterization of Anatase/Rutile–TiO_2 Thin Films by Magnetron Sputtering: A Review. *Sci. Technol. Adv. Mater.* **2005**, *6*, 11–17. [CrossRef]
65. Sun, X.W.; Kwok, H.S. Optical Properties of Epitaxially Grown Zinc Oxide Films on Sapphire by Pulsed Laser Deposition. *J. Appl. Phys.* **1999**, *86*, 408–411. [CrossRef]
66. Lee, G.H.; Kawazoe, T.; Ohtsu, M. Difference in Optical Bandgap between Zinc-Blende and Wurtzite ZnO Structure Formed on Sapphire (0001) Substrate. *Solid State Commun.* **2002**, *124*, 163–165. [CrossRef]
67. Popov, A.P.; Zvyagin, A.V.; Lademann, J.; Roberts, M.S.; Sanchez, W.; Priezzhev, A.V.; Myllylä, R. Designing Inorganic Light-Protective Skin Nanotechnology Products. *J. Biomed. Nanotechnol.* **2010**, *6*, 432–451. [CrossRef]
68. Behnajady, M.A.; Modirshahla, N.; Shokri, M.; Elham, H.; Zeininezhad, A. The Effect of Particle Size and Crystal Structure of Titanium Dioxide Nanoparticles on the Photocatalytic Properties. *J. Environ. Sci. Health A* **2008**, *43*, 460–467. [CrossRef] [PubMed]